Supporting Information

Feldman et al. 10.1073/pnas.1413640111

Modeling Spectral Emissivity of Different Surface Types

i) For ocean surfaces, angularly integrated spectral emissivity is computed using the refractive index of liquid water from Hale and Querry (1) and the Fresnel equation (2). Fig. S1 shows the comparison of modeled and measured spectral emissivity of a water surface. Note that all surface spectral emissivities archived by the ASTER Spectral Library (speclib.jpl.nasa.gov/) (3) stop at 650 cm^{-1}. This database incorporates no far-IR measurements, and comparisons with data can be only made for the mid-IR.

ii) For snow surfaces, the methodology follows Chen et al. (4). Mie scattering theory is used to compute the optical properties of snow with a range of diameters from 300 μm to 1,100 μm and a median value of 600 μm (5). The index of refraction of ice is taken from Warren and Brandt (6). Then the optical properties are corrected for densely packed particles by applying a structure correction factor (7, 8). The corrected optical properties are then fed into a Hapke model (9) for simulating hemispherical mean (angularly averaged) emissivity. Fig. S2 shows the simulated and measured directional snow emissivity at viewing zenith angle of 45°.

iii) For desert surfaces, the spectral emissivity is computed in a similar way to that of ocean surfaces. First, angularly averaged emissivities of minerals commonly seen in the desert soil are modeled. These minerals include Montmorillonite (SWy-1), Beidellite (SBld-1), Nontronite (NAu-1), Hectorite (SHCa-1), Saponite (SpNv-1), Illite (IMt-1), Illite-Smectite (IsMt-1), Kaolinite (KGa-1), Halloysite (HWw-1), and Serpentine (BUR-1690). The index of refraction is taken from Glotch et al. (10). Note that these minerals have similar chemical compositions, and that is why their spectral emissivities are similar. Then we use the average of these spectral emissivities to represent the mean spectral emissivity of desert surfaces. Fig. S3 shows the measured and modeled spectral emissivity for each mineral used here.

iv) For vegetation, the ASTER spectral library provides spectral emissivity of three live leaves (grass, conifer, and deciduous) measured at 60° viewing zenith angle. Given the lack of index of refraction information of leaves and the fact that 60° is close to the diffusive angle of 52°, we simply use the mean spectral emissivity of the three live leaves from ASTER library to approximate the angularly averaged emissivity. Also, given that the spectral emissivity of leaves has less frequency dependence in the longwave than spectral albedo has in the shortwave, the far-IR emissivity is simply assumed to be the same as that at the longest mid-IR wavelength (i.e., the smallest wavenumber) in the ASTER spectral library.

Global Surface Band-by-Band Emissivity

For the aforementioned four surface types, the spectral emissivity of each surface type is first averaged onto the emissivity of each individual band used by RRTMG, i.e., 16 IR bands in total. Then the surface type of each CESM grid is determined from the 1-km resolution land coverage dataset from the US Geological Survey (11), which has 18 different surface types following the definition of the International Geosphere-Biosphere Program (IGBP) surface classification, with one additional type of tundra. For IGBP type 17 over an ocean surface, the water spectral emissivity is used; for IGBP type 15, snow spectral emissivity is used; for IGBP types 6, 7, and 16 (desert surfaces), the emissivity of desert is used; for all other land surfaces, we assume they are vegetated surfaces. A sample map of band-by-band and band-averaged far-IR surface emissivity used in RRTMG is shown in Fig. S4.

CESM Modification

Currently, the treatment of emissivity is very simplistic in CESM. The implementation in RRTMG assumes that emissivity is 1.000 at all wavelengths. However, the radiative surface temperature that is passed to RRTMG contains a representation of surface emissivity derived from other model components. Specifically, please refer to the Description of the National Centers for Atmospheric Research Community Atmosphere Model (CAM 5.0) (NCAR/TN-486+STR), November 2012 (www.cesm.ucar.edu/models/cesm1.0/cam/docs/description/cam5_desc.pdf), Section 4.10.4 (page 170), which states:

> "In the longwave, the surface is assumed to have an emissivity of 1.0 within the radiation model. However, the radiative surface temperature used in the longwave calculation is derived with the Stefan-Boltzmann relation from the upward longwave surface flux that is input from the surface models. Therefore, this value may include some representation of surface emissivity less than 1.0, if this condition exists in surface models (e.g. the land model)."

A closer inspection of other components of CESM 1.0.5 yields the following. In the land model, emissivity is spectrally gray and is set by the following: snow emissivity is set to 0.97 (in Biogeophysics1Mod.F90), nonurban ground emissivity is 0.97 (in UrbanMod.F90), and urban ground emissivity is 0.96 (in UrbanMod.F90). Vegetation emissivity is set by the following expression:

$$\varepsilon_{veg} = 1 - e^{-\frac{(\mathrm{LAI}+\mathrm{SAI})}{\tau_{leaf}}},$$

where LAI is the leaf area index, SAI is the stem area index, and τ_{leaf} is the infrared inverse optical depth per unit leaf area (in Biogeophysics1Mod.F90). In the Ocean model, emissivity is set to 1.000 (in constants.F90). In the Ice model, emissivity of snow and ice are set to 0.98.

The disparate treatment of surface emissivity across the components of CESM is apparent along with the lack of any ability to specify spectral dependence outside of the Atmosphere model.

In our modification to CESM, we passed arguments of latitude, longitude, land snow fraction, sea ice fraction, and fractional land coverage to RRTMG and calculate far-IR emissivity based on a weighted average of scene types within a given grid box. RRTMG contains three bands across the far infrared: 10–250 cm^{-1}, 250–500 cm^{-1}, and 500–630 cm^{-1}, and so we averaged scene-type surface emissivity over those bands (i.e., our specification was not spectrally gray).

1. Hale GM, Querry MR (1973) Optical constants of water in the 200 nm to 200 μm wavelength region. *Appl Opt* 12(3):555–563.
2. Masuda K, et al. (1988) Emissivity of pure and sea waters for the model sea surface in the infrared window regions. *Remote Sens Environ* 24(2):313–329.
3. Baldridge AM, et al. (2009) The ASTER Spectral Library version 2.0. *Remote Sens Environ* 113(4):711–715.
4. Chen X, et al. (2014) Sensitivity of modeled far-IR radiation budgets in polar continents to treatments of snow surface and ice cloud radiative properties. *Geophys Res Lett* 41:6530–6537.
5. Hori M, et al. (2006) In-situ measured spectral directional emissivity of snow and ice in the 8–14 μm atmospheric window. *Remote Sens Environ* 100(4):486–502.
6. Warren SG, Brandt RE (2008) Optical constants of ice from the ultraviolet to the microwave: A revised compilation. *J Geophys Res* 113(D14):D14220.
7. Mishchenko MI (1994) Asymmetry parameters of the phase function for densely packed scattering grains. *J Quant Spectrosc Radiat Transfer* 52(1):95–110.
8. Mishchenko MI, Macke A (1997) Asymmetry parameters for the phase function for isolated and densely packed spherical particles with multiple internal inclusions on the geometric optics limit. *J Quant Spectrosc Radiat Transfer* 57(6):767–794.

9. Hapke B (1993) *Theory of Reflectance and Emittance Spectroscopy* (Cambridge Univ. Press, New York).
10. Glotch TD, Rossman GR, Aharonson O (2007) Mid-infrared (5–100 μm) reflectance spectra and optical constants of 10 phyllosilicate minerals. *Icarus* 192(2):605–662.
11. Loveland TR, et al. (2000) Development of a global land cover characteristics database and IGBP DISCover from 1 km AVHRR data. *Int J Remote Sens* 21(6-7):1303–1330.

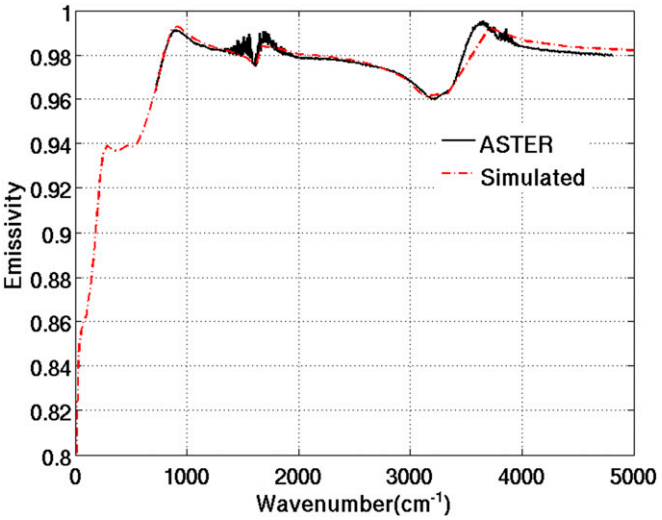

Fig. S1. Simulated water emissivity (red line) and ASTER measured emissivity (black line) at viewing zenith angle = 10°.

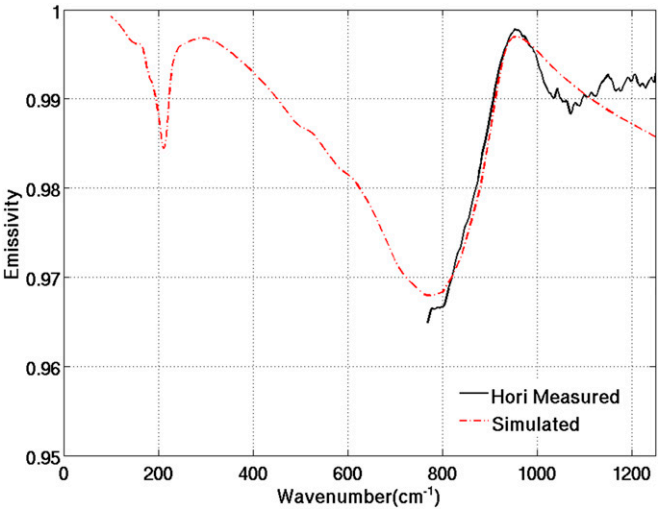

Fig. S2. Simulated snow emissivity (red line) and measured emissivity by Hori et al. (5) (black line) at viewing zenith angle = 45°.

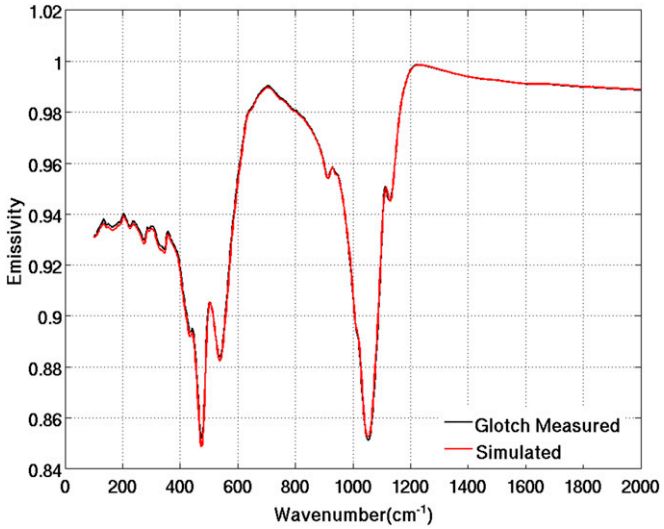

Fig. S3. Mean spectral emissivity averaged over the ten minerals mentioned above as measured by Glotch et al. (10) (black line) at viewing zenith angle = 20° and as simulated (red line).

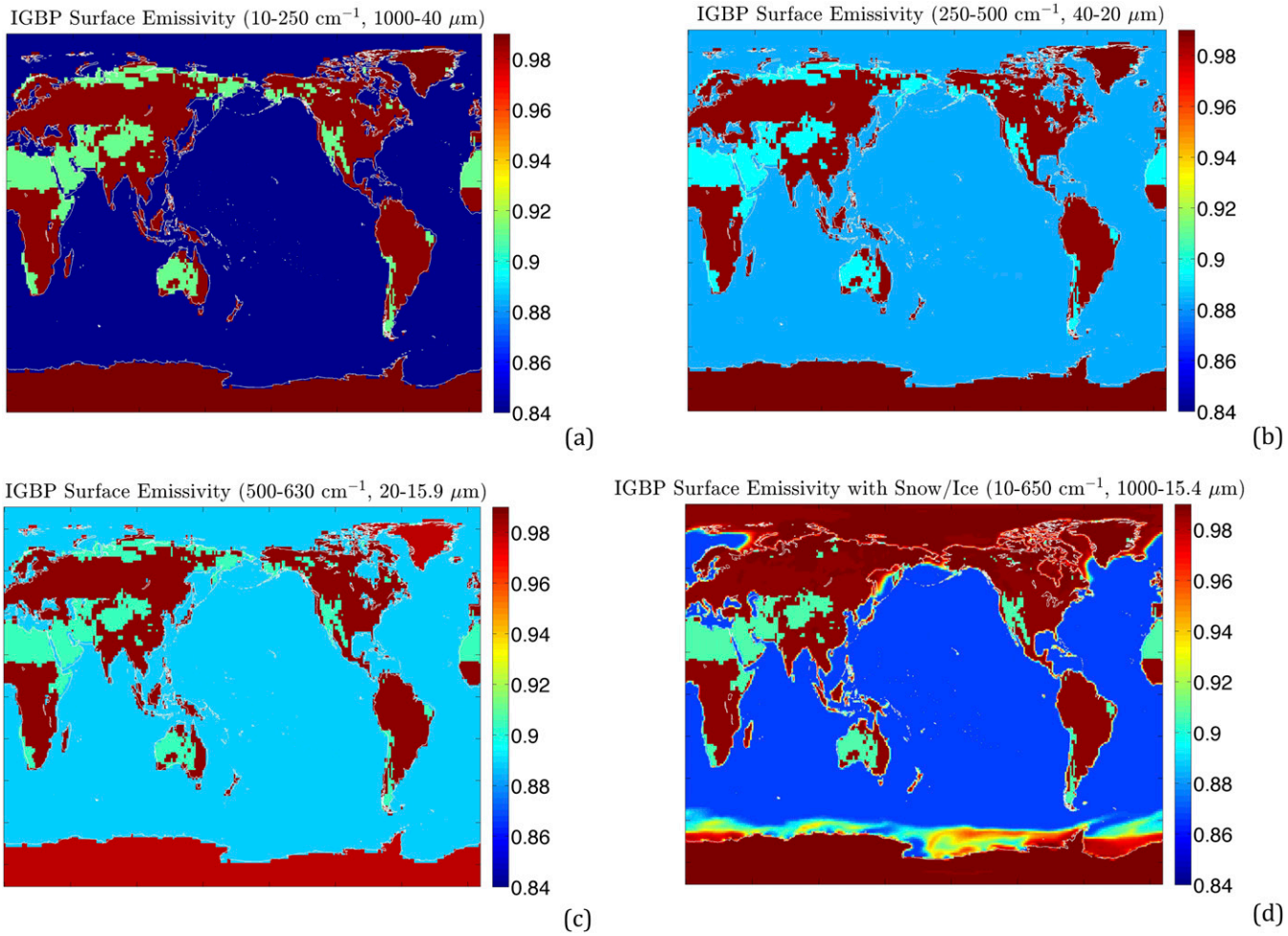

Fig. S4. Maps of surface emissivity from IGBP surface types for (*A*) 10–250 cm^{-1} without considering frozen surface extent. (*B*) Same as *A* but for a frequency range of 250–500 cm^{-1}. (*C*) Same as *A* but for a frequency range of 500–630 cm^{-1}. (*D*) Far-IR average emissivity (10–650 cm^{-1}) including frozen surface coverage as determined from CESM running RCP8.5 for the month of January 2005.